PROCEEDINGS OF SPIE

SPIEDigitalLibrary.org/conference-proceedings-of-spie

Secure optical layer flexibility in 5G networks

Mingwei Yang, Houman Rastegarfar, Ivan B. Djordjevic

Mingwei Yang, Houman Rastegarfar, Ivan B. Djordjevic, "Secure optical layer flexibility in 5G networks," Proc. SPIE 11048, 17th International Conference on Optical Communications and Networks (ICOCN2018), 1104814 (14 February 2019); doi: 10.1117/12.2519926

SPIE.

Event: 17th International Conference on Optical Communications and Networks (ICOCN2018), 2018, Zhuhai, China

Secure Optical Layer Flexibility in 5G Networks

Mingwei Yang *[a], Houman Rastegarfar[b], and Ivan B. Djordjevic[a]
[a]Dept. of Electrical and Computer Engineering, The University of Arizona, Tucson, AZ 85721, USA; [b]College of Optical Sciences, The University of Arizona, Tucson, AZ 85721, USA

ABSTRACT

We propose an adaptive resource allocation framework for on-demand communications in a software-defined mobile fronthaul (MFH) network that supports dynamic processing resource sharing. Our theoretical and experimental studies point to the feasibility of secure bidirectional transmission with guaranteed bit error rate (BER) service using adaptive modulation and coding.

Keywords: Adaptive modulation and coding; arrayed waveguide grating (AWG); mobile fronthaul (MFH); preamble encoding; software-defined networking (SDN).

1. INTRODUCTION

Compared to the existing cellular networks, the fifth-generation cellular networks (5G) should support 1,000 times higher traffic rates, up to 100 times more connection density, millisecond-scale latencies, and up to 10 Gb/s stationary access rates [1]-[3]. These dramatic performance enhancements call for innovations in multiple technology domains, including network architecture, control, and signal processing. From a network architecture point of view, the densification of radio access points and the centralization of baseband processing functions are two major trends that should be included in 5G implementations. To this end, the centralized radio access network (C-RAN) architecture has been introduced to support heterogeneous cell types in a cost- and power-efficient fashion. In a C-RAN, base stations are split into baseband processing units (BBUs) and remote radio heads (RRHs), where the BBUs are pooled in a central office for statistical multiplexing and high-gain coordinated multipoint (CoMP) services. The interface between the BBU pool and the RRHs is known as the mobile fronthaul (MFH) network. The multiplicity of the radio nodes and the capacity and latency requirements imposed by wireless coordination schemes and standards such as the Common Public Radio Interface (CPRI) pose significant challenges to the design of MFH networks [4]-[7].

Despite the immense capacity of optical fiber networks, a static optical MFH network with dedicated, rigid BBU-RRH connections of fixed capacity is not desirable due to the prohibitive costs of resource overprovisioning. Fortunately, software-defined networking (SDN) provides for physical layer programmability in optical networks based on a logically centralized network controller. By properly extending OpenFlow, i.e., the predominant SDN southbound interface protocol, it is now feasible to support highly dynamic optical switching scenarios, taking into account both application layer requirements and physical layer conditions [8],[9]. With SDN control, it is feasible to conduct cross-layer resource allocation and performance optimization in MFH networks. Based on an application's bit rate and service latency requirements as well as the signal quality measures reported from the physical layer, the SDN controller can optimize the resources allocated to the application in terms of carrier frequency, transmit power, modulation type/order, and forward error correction (FEC) code type/rate, etc. Resource adaptability in the physical layer results in a highly flexible system, improving the scalability, cost, and power consumption of the MFH network [10]-[12]. An adaptation scheme in the optical network, however, should be carefully implemented in order not to compromise the security of the wireless side [13].

In this paper, we combine SDN control, wavelength routing, and physical-layer resource adaptation based on pulse amplitude modulation (PAM) and low-density parity-check (LDPC) coding to achieve a highly flexible and resource-efficient MFH network, supporting real-time reconfiguration on both switch architecture and transceiver levels. Using an arrayed waveguide grating (AWG)-based switch fabric and tunable transceivers in the nodes, we enable the programmable and highly secure connectivity of BBU and RRH terminals in both downlink and uplink scenarios. Compared to time- and wavelength-division multiplexed (TWDM) approaches in traditional passive optical networks, we make use of self-generated pseudorandom sequences to achieve "any RRH to any BBU" bidirectional communications with wide covered distances, energy efficiency, and service security. Our cross-

17th International Conference on Optical Communications and Networks (ICOCN2018),
edited by Zhaohui Li, Proc. of SPIE Vol. 11048, 1104814 · © 2019 SPIE
CCC code: 0277-786X/19/$18 · doi: 10.1117/12.2519926

layer resource allocation involves several modifications to standard SDN implementations, which are introduced as extension modules.

2. SDN-ENABLED BIDIRECTIONAL TRANSMISSION SCHEME

To achieve a highly flexible MFH, we consider a wavelength-routing architecture with broadcast capabilities [14]. According to Fig. 1 (depicting both downstream and upstream transmission scenarios), the BBUs are connected to multiple input ports of an AWG using star couplers. Along with the cyclic routing pattern of the AWG [15], these couplers enable the BBUs to be assigned to different wireless domains without any blocking. Different AWG output ports provide service to distinct geographical domains (e.g., residential, business). The power splitters support traffic multicasting among the RRHs within a domain. Tunable filters (TFs) are employed to select the signal from the desired BBU port. We utilize optical circulator for bidirectional communications. By pooling all the BBU resources in a central office, this design supports statistical multiplexing. Hence, the number of BBUs can be significantly smaller than the number of RRHs in the system.

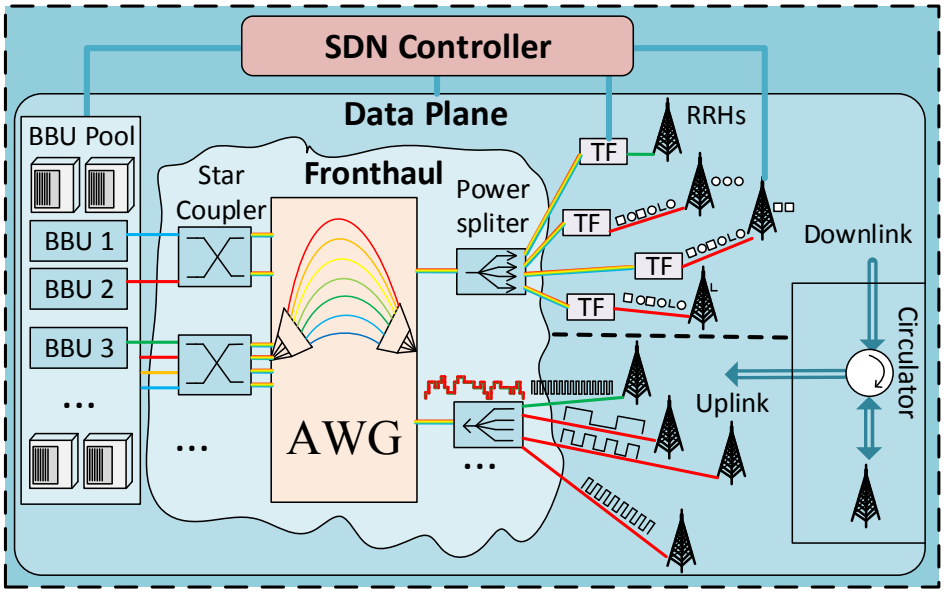

Figure 1. MFH network architecture based on wavelength routing.

Code-division multiple access (CDMA) has potential for capacity upgrade in optical MFH networks [16]. We consider pseudorandom (PR)-preamble encoding for downlink [17],[18], and code division multiplexing for uplink transmission. Both of these coding schemes support resource adaptation in addition to node synchronization. From a physical layer standpoint, the transfer of information from a BBU to an RRH is in the form of a sequence of frames, each comprising a payload and a PR-preamble. To provide for adaptive data rate per connection, the physical layer parameters (e.g., modulation order, code rate, and transmit power) are chosen by the SDN controller and encoded into the preamble in the form of a pseudorandom bit sequence (PRBS) unique to each connection. As other nodes are oblivious of the PRBS content, secure communications is ensured in addition to physical-layer synchronization and rate adaptation. The transceiver parameters can be adjusted dynamically based on the variations in the communication channel's properties or the mobile application needs.

Figure 2 depicts the MFH SDN control plane architecture and the SDN-enabled preamble encoding/decoding procedure. Building on the OpenFlow protocol, we implemented extension modules to support the MFH adaptive modulation and coding functions. These include the pre- FEC bit error rate (BER) monitor, routing and wavelength assignment (RWA), code and modulation selection (CMS), and transmission configuration (TC) modules. The RWA module is intended for setting up a fronthaul connection between a BBU and an RRH by properly controlling the tunable hardware. Once the connection has been established, the receiver reports the pre-FEC BER to the BER monitor. Based on the reported value and the target post-FEC BER, a lookup table in the

CMS module is employed to determine the proper modulation order and code type. Finally, the TC module encodes the physical layer parameters onto a PRBS preamble, which is generated in real time.

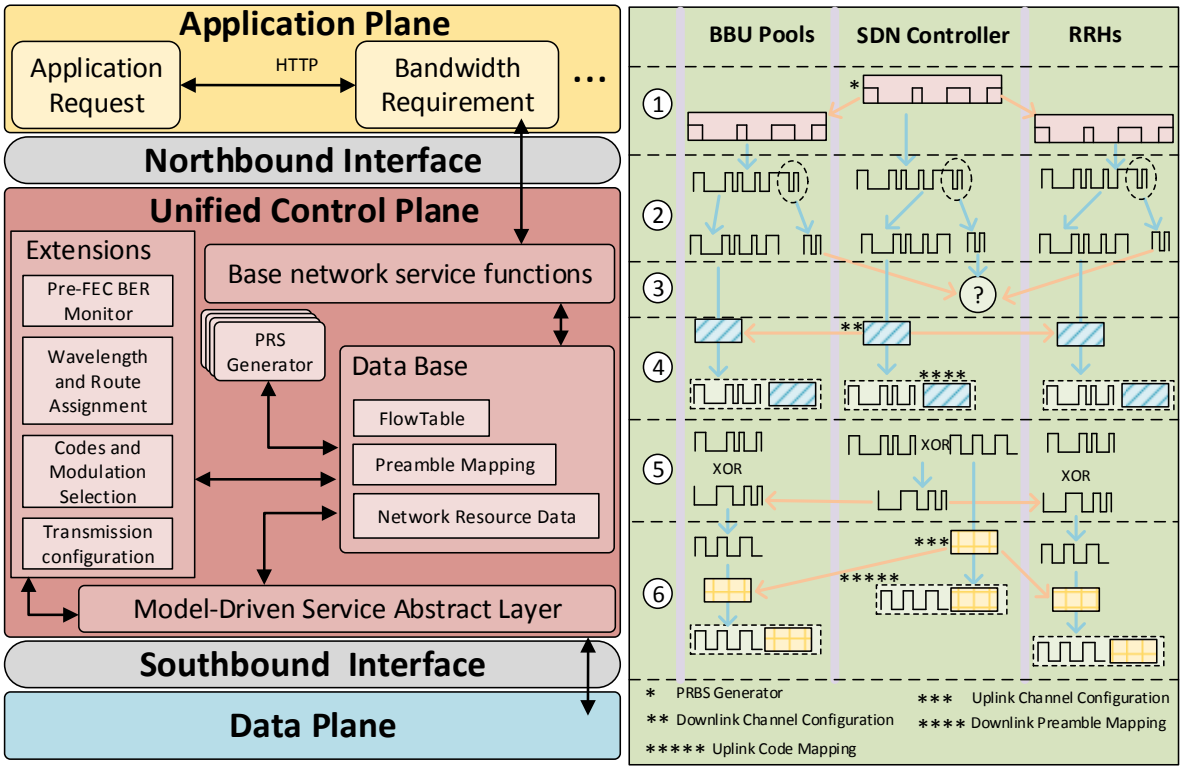

Figure 2. (left) SDN controller architecture, (right) steps involved in the secure encoding/decoding operations.

As in Fig. 2, the PRBS generator at the transmitter node is initialized with the seed obtained from the controller. The same seed is also passed to the recipient of the encoded and modulated data. This enables the same preamble to be generated by the SDN controller, the source node, and the destination node. Using a cross-correlation operation, the receiver detects and decodes the preamble, leading to frame synchronization and the detection of the demodulation and decoding parameters. The process involving the secure distribution of codes among BBU and RRH nodes comprises six steps.

1) Prior to setting up the connection, the SDN controller synchronizes the status of the PRBS generators involved.
2) Each PRBS generator generates a long PR code for preamble encoding as well as a short code.
3) The SDN controller sees whether the long codes are identical in the BBU and the RRH by collecting and comparing the short codes.
4) The controller assigns the downlink configuration parameters (e.g., modulation order, LDPC code, and frame length) to the BBU and the RRH and implements the preamble-configuration mapping.
5) The controller selects the spreading code for uplink transmission and calculates a complementary code with an XOR operation. It sends the complementary code to the RRH and the BBU.
6) The BBU and the RRH calculate the correct spreading code based on an XOR operation. The length of the spreading code is determined by the length of the complementary code. The controller assigns the uplink configuration parameters to the BBU and the RRH and completes the mapping.

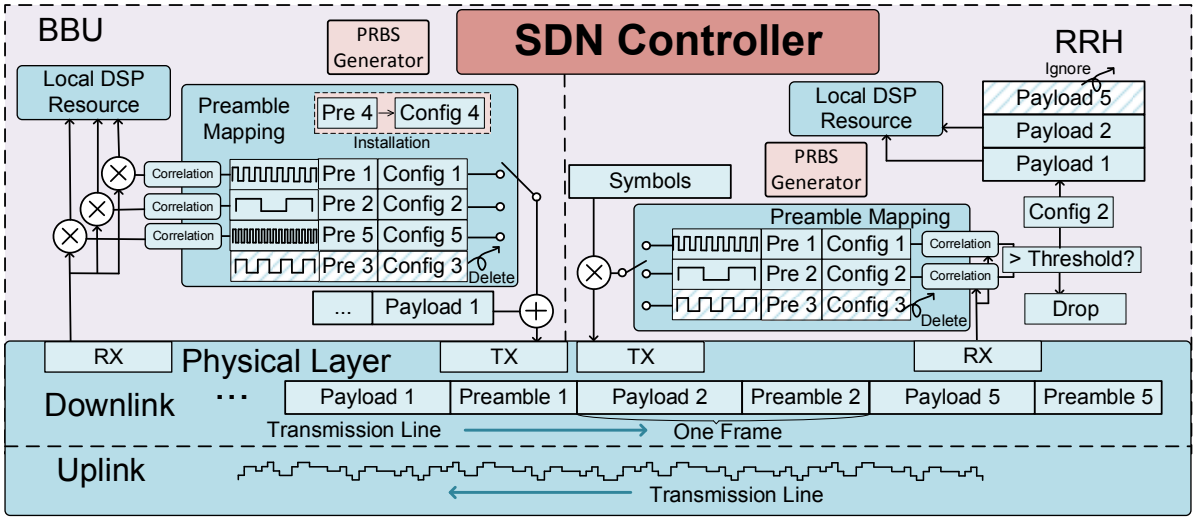

Figure 3. SDN-enabled preamble encoding (downlink) and code division multiplexing (uplink).

Figure 3 depicts the SDN control-data plane interfaces for preamble encoding and code division multiplexing. The collaboration of the MFH nodes with the SDN controller ensures that code-configuration mapping can take place with very high reliability. Since a receiver can detect several codes simultaneously, the transmitter can switch the configuration parameters dynamically and without any time gap. Moreover, it is not necessary to repeat the synchronization step for generating a new mapping. By refraining from disseminating the actual preamble and spreading codes, both uplink and downlink transmissions are highly secure in the physical layer.

3. EXPERIMENTAL AND THEORETICAL VALIDATION

We report experimental and theoretical results on the downlink and uplink transmission performance, respectively. Figure 4 depicts our downlink experimental setup. At the transmitter side, four 10 kHz-linewidth, continuous-wave, tunable lasers (with λ_1:193.40 THz, λ_2: 193.30 THz, λ_3: 193.35 THz, and λ_4: 193.20 THz) are combined two by two and applied to two Mach-Zehnder modulators. The binary data sequence is adaptively encoded using LDPC codes (n, k, R, g), where n, k, R, and g denote the codeword length, information word length, code rate, and the girth of the corresponding bipartite graph representation of the parity-check matrix, respectively [19]. We consider two codes, namely, code 1: (16935, 13550, 0.8, 8) and code 2: (18488, 11557, 0.625, 10). The encoded bits are mapped to M-level PAM symbols and are pulse shaped by two arbitrary waveform generators (AWGen) to generate 25 GBaud PAM-2 (OOK) and PAM-4 signals. The resulting signals are amplified by an erbium-doped fiber amplifier (EDFA) with a 6 dB noise figure and then applied to an AWG-based MFH network. Fibers of different length are placed between the input-stage couplers and the AWG to interleave the signals. At the AWG output, signals are broadcast to receivers via couplers. Optical variable attenuators (OVA) are employed before RRHs to emulate the power loss due to different propagation distances. The optical power per wavelength is set to -5 dBm at the receiver with 0 dB attenuation.

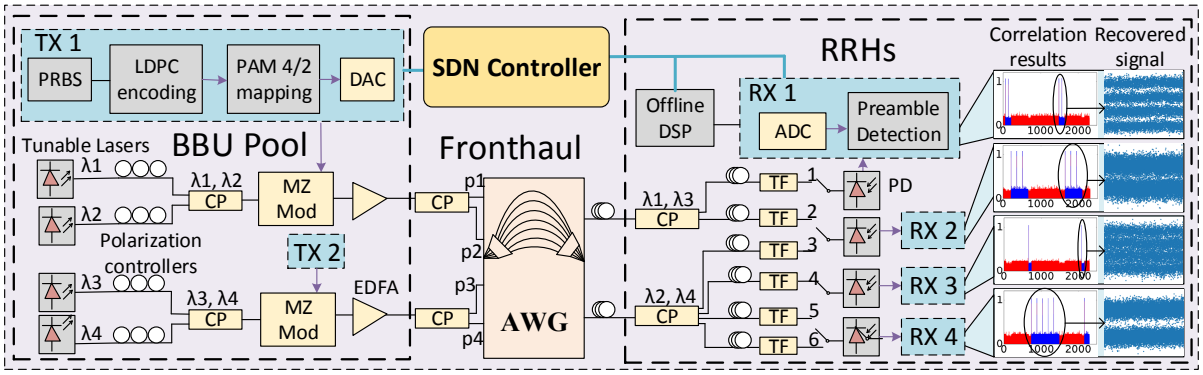

Figure 4. Downlink transmission experimental setup (CP: coupler, PD: photodetector, ADC: analog-to-digital converter, DAC: digital-to-analog converter).

To assess the feasibility of on-demand BBU-RRH connectivity, we considered different wavelength configurations for unicast and multicast transmission. Figure 4 illustrates one such configuration with the real-time detection outcome and the recovered signals on the right-hand side. Since different distances and routes are emulated, received signals experience different signal-to-noise ratio (SNR) conditions. The blue portion of the correlation graphs denote the sequence of frames intended to the corresponding RRH, whereas the red portion is disposed of without detection since it belongs to other RRHs. The peak values mark successful preamble detection instances based on cross-correlation operation.

The downlink post-FEC BER performance achieved with code rate adaptation for PAM-2 and PAM-4 is depicted in Fig. 5. The values on the horizontal axes correspond to the distance between an RRH and the AWG output (i.e., the distance from the central office to the antenna site). The distances are calculated based on the attenuation coefficient of a standard single-mode optical fiber (0.2 dB/km). Each curve is associated with a label of form P*MCn_l*ax, where *M* is the PAM order, *n* indicates the code type, and *l* denotes the number of adjacent AWG input ports that carry signal. Depending on the wavelength of the adjacent signals, in-band and/or out-of-band crosstalk could develop and affect the BER of the desired signal.

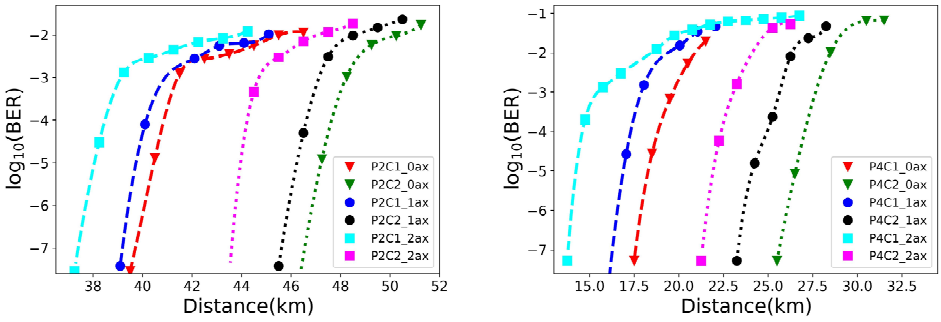

Figure 5. Downlink code rate adaptation performance under (left) PAM-2 and (right) PAM-4.

We define cover range, CR, as the range of distances that can support a target post-FEC BER. A larger value of CR points to the possibility of supporting RRHs more flexibly. For example, CR=0 implies that all RRHs should experience the same physical conditions (in terms of distance, impairment, etc.) to receive service from the MFH network. According to Fig. 5, for a post-FEC BER=10^{-7}, LDPC code rate adaptation allows for a cover range of 9 km for PAM-2 and 12 km for PAM-4. Combining adaptive coding with adaptive modulation, CR can reach a value as large as 34 km (i.e., the difference between the maximum distance supported with PAM-2 and the minimum distance supported with PAM-4), pointing to the remarkable flexibility that can be achieved with adaptation in the physical layer. In terms of MFH connection net transmission rate, CR=9 km (with PAM-2) translates to data rates in the range of (15.625,20) Gb/s, considering the choice of symbol rate and code types. With CR=12 km, the range of supported data rates is (31.25,40) Gb/s. With CR=34 km (both modulation order and code rate adaptation), a much wider range of (15.625,40) Gb/s is achieved. While our experiments involve only two code types and two modulation orders, the number of code rates and modulation orders can be adjusted for the desired fronthaul service granularity.

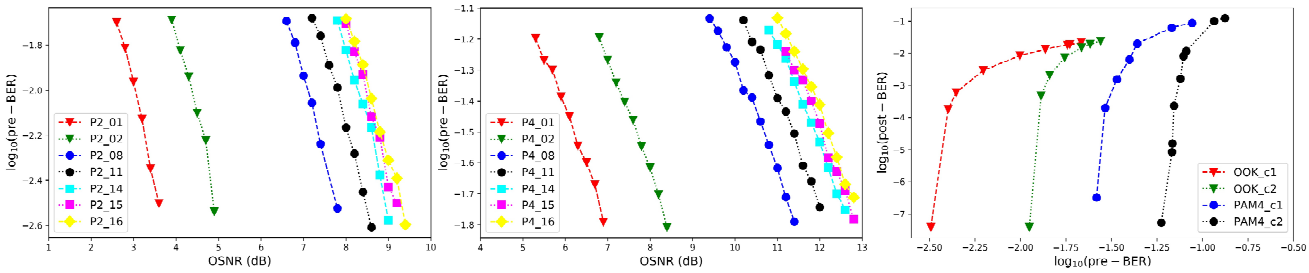

Figure 6. Uplink pre-FEC BER versus OSNR for (left) PAM-2 and (middle) PAM-4. (right) Relation of post-FEC and pre-FEC BER for different modulation orders and code types.

For studying the uplink transmission performance in our MFH architecture, we simulate a CDMA network employing a 16-bit Walsh-Hadamard code as the spreading code set [20]. The system is operated under the additive white Gaussian noise (AWGN) channel assumption, with a laser wavelength of 1550 nm, linewidth of 100 KHz, and optical power of 10 dBm. The sampling rate is 50 GS/s with four samples per symbol. We simulate the scenarios with 1, 2, 8, 11, 14, 15, and 16 users (i.e., RRHs). The power of signal and noise are equal before being combined together. Each RRH's code is synchronized with a random misalignment of less than 0.25 times the symbol rate.

In a CDMA system, the performance is mainly affected by multi-user interference as well as Gaussian noise from each user. Considering PAM, the pre-FEC BER versus optical signal-to-noise ratio (OSNR) for different number of active RRHs is depicted in Fig. 6. The theoretical results indicate that the number of active RRHs has a notable impact on the uplink transmission performance. With the same noise level, more RRHs will lead to higher pre-FEC BER at the BBU pool site. In a practical setting, the SDN controller should maintain the number of active RRHs with a small fluctuation. Comparing the pre-FEC BER values with 11, 14, 15, and 16 active RRHs, one can infer that adaptive LDPC coding can satisfy the quality of service with a guaranteed post-FEC BER.

Finally, to fully demonstrate the potential of adaptive modulation and coding in MFH networks, we consider two LDPC codes (i.e., codes 1, 2) with code rates of 0.8 and 0.625 and two modulation orders. Figure 6 depicts the post-FEC BER performance as a function of the modulation order and pre-FEC BER. The results suggest that with adaptive modulation and coding it is feasible to guarantee a post-FEC BER of 10^{-7} with pre-FEC BER ranging from $10^{-1.6}$ to $10^{-1.2}$ for PAM-4 and $10^{-2.5}$ to $10^{-1.95}$ for OOK.

4. CONCLUSION

We proposed a secure SDN-enabled optical fronthaul resource allocation scheme, enabling the bidirectional connectivity of any BBU to any RRH by taking into account the physical-layer conditions. We experimentally verified the advantages of adaptive coding and modulation in an MFH downlink scenario based on preamble encoding. Compared to a worst-case overprovisioning scenario, physical-layer adaptation could lead to performance gains as large as 156% in terms of the maximum achievable data rate. Besides, our theoretical study of the uplink transmission performance indicated the benefits of adaptive modulation and coding for maintaining the required post-FEC BER. In the future, we will assess the uplink transmission performance experimentally and will also implement the control and signal processing modules in an FPGA board for optimized speed and power consumption. Furthermore, we plan to examine the impact of asynchronous CDMA and dynamic length spreading code for the uplink system.

REFERENCES

[1] P. K. Agyapong, M. Iwamura, D. Staehle, W. Kiess, and A. Benjebbour, "Design considerations for a 5G network architecture," IEEE Commun. Mag., vol. 52, no. 11, pp. 65-75, Nov. 2014.

[2] A. Tzanakaki et al., "Wireless-optical network convergence: enabling the 5G architecture to support operational and end-user services," IEEE Commun. Mag., vol. 55, no. 10, pp. 184–192, Oct. 2017.

[3] F. Z. Yousaf, M. Bredel, S. Schaller, and F. Schneider, "NFV and SDN–key technology enablers for 5G networks," IEEE J. Sel. Areas Commun., vol. 35, no. 11, pp. 2468–2478, Nov. 2017.

[4] M. R. Raza et al., "Demonstration of dynamic resource sharing benefits in an optical C-RAN," IEEE. J. Opt. Commun. Netw, vol.8, no. 8, pp. 621-632, Aug. 2016.

[5] J. Zhang et al., "Reconfigurable optical mobile fronthaul networks for coordinated multipoint transmission and reception in 5G," J. Opt. Commun. Netw, vol. 9, no. 6, pp. 489-497, Jun. 2017.

[6] H. Rastegarfar, T. Svensson, and N. Peyghambarian, "Reliability gains of infrastructure programmability in an optical C-RAN," Proc.Opt. Fiber Commun. Conf., San Diego, USA, Mar. 2018, paper Th2A.40.

[7] K. Zhang et al., "Low-cost WDM fronthaul enabled by partitioned asymmetric AWGR with simultaneous flexible transceiver assignment and chirp management," IEEE J. Opt. Commun. Netw., vol. 9, no. 10, pp. 876–888, Oct. 2017.

[8] H. Rastegarfar et al. "TCP flow classification and bandwidth aggregation in optically interconnected data center networks," IEEE. J. Opt. Commun. Netw., vol. 8, no. 10, pp. 777-786, Oct. 2016.

[9] M. Yang et al, "Traffic-aware non-uniform passband assignment in elastic optical networks," Proc. IEEE Photonics Conf., Reston, USA, Oct. 2015, pp. 402-403.
[10] F. Lu et al., "Adaptive digitization and variable channel coding for enhancement of compressed digital mobile fronthaul in PAM-4 optical links," J. Lightw. Technol., vol. 35, no. 21, pp. 4714-4720, Nov. 2017.
[11] M. Yang, H. Rastegarfar, and I. B. Djordjevic, "SDN-enabled cross-layer flexibility in 5G fronthaul networks," Proc. European Conf. on Opt. Commun., Rome, Italy, Sep. 2018 (accepted).
[12] M. Yang, H. Rastegarfar, and I. B. Djordjevic, "Secure bidirectional adaptive resource allocation in SDN-enabled 5G fronthaul networks," Proc. Asia Commun. and Photon. Conf. (ACP), Hangzhou, China, Oct. 2018 (submitted).
[13] John Gariano and I. B. Djordjevic, "Multimode entanglement assisted QKD through a free-space maritime channel," Quantum Information Science and Technology III, vol. 10442, 2017, paper 104420B.
[14] H. Rastegarfar, L. A. Rusch, and A. Leon-Garcia, "Optical load-balancing tradeoffs in wavelength-routing cloud data centers," IEEE J. Opt. Commun. Netw., vol. 7, no. 4, pp. 286-300, Apr. 2015.
[15] H. Rastegarfar, L. Yan, K. Szczerba, and E. Agrell "PAM performance analysis in multicast-enabled wavelength-routing data centers," J. Lightw. Technol., vol. 35, no. 13, pp. 2569-2579, Jul. 2017.
[16] M. Hadi and M. R. Pakravan, "Analysis and design of adaptive OCDMA passive optical networks," J. Lightw. Technol., vol. 35, no. 14, pp. 2853-2863, Jul. 2017.
[17] M. Yang, H. Rastegarfar, and I. B. Djordjevic, "SDN-based application driven in-band adaptive coding in data centers," Proc.Opt. Fiber Commun. Conf., San Diego, USA, Mar. 2018, paper W2A.21.
[18] M. Yang and I. B. Djordjevic, "SDN-based in-band adaptive synchronization with self-generated preamble detection scheme," Proc. Asia Communications and Photonics Conf., Guangzhou, China, Nov. 2017, paper Su4B.5.
[19] Z. Qu et al., "Performance optimization of PM-16QAM transmission system enabled by real-time self-adaptive coding," Opt. Lett., vol. 42, no. 20, pp. 4211-4214, Oct. 2017.
[20] K. J. Horadam, Hadamard matrices and their applications, Princeton University Press, 2012.